Cold plasma assisted synthesis of spinel-CoFe_2O_4 nanoparticle with narrow bandgap and high magnetic activity

Harshini Mohan, Subash Mohandoss, Aparna Prakash, Natarajan Balasubramaniyan, Sivachandiran Loganathan, Aymen Amin Assadi, Ahmed Khacef

Cold plasma Assisted Synthesis of spinel-$CoFe_2O_4$ Nanoparticle with Narrow Bandgap and high Magnetic Activity

Harshini MOHAN[1], Subash MOHANDOSS[1], Aparna PRAKASH[1], Natarajan BALASUBRAMANIYAN[1], Sivachandiran LOGANATHAN[1,2*], Aymen Amin ASSADI[3,4] , Ahmed KHACEF[5]

[1]Laboratory of Plasma Chemistry and Physics (LPCP), Department of Chemistry, Faculty of Engineering and Technology, SRM Institute of Science and Technology, Kattankulathur – 603203, Chengalpattu District, Tamil Nadu, India.
[2]Center for Air and Aquatic Resources Engineering & Science, Department of Civil and Environmental Engineering, Clarkson University, Potsdam, New York 13699, United States.
[3]College of Engineering, Imam Mohammad Ibn Saud Islamic University (IMSIU), P.O. Box 5701, Riyadh 11432, Saudi Arabia
[4]Univ Rennes – ENSCR-11, Alée de Beaulieu – CS 50837 - 35708 Rennes Cedex 7, France.
[5]GREMI, CNRS-Université d'Orléans, 14 Rue D'Issoudun, 45067, Orléans, France

ABSTRACT

Non-thermal plasma (NTP)-assisted catalysis offers a promising avenue with diverse applications, particularly in air and water treatment. This study aimed to investigate the utilization of NTP discharge for the synthesis of magnetically active nanoparticles (MANps). We have demonstrated that the NTP discharge-assisted low-temperature calcination effectively induces surface modification and crystallization, thereby enhancing magnetic susceptibility. Specifically, a 30 min plasma treatment at 200°C (CF-P-200) facilitated the formation of crystalline particles, a phenomenon that was absent in materials synthesized without plasma treatment under similar operating conditions. High-resolution microscopy revealed an average particle size of about 6.7 nm, while EDX analysis unveiled surface oxygen defects in CF-P-200 compared to materials synthesized by conventional calcination at 600°C (CF-T-600), resulting in a narrower bandgap (1.9 eV). Magnetization measurements conducted using vibrating sample magnetometry (VSM) displayed superior magnetic properties of plasma treated MANps, with a magnetization (Ms) of 91.80 emu/g and coercivity (Hc) of 888 Oe. These values outperformed those of materials calcined at 600°C (Ms: 64.53 emu/g, Hc: 1289 Oe), emphasizing the efficacy of NTP discharge in enhancing magnetic characteristics during material synthesis.

Key words: Non-thermal plasma, $CoFe_2O_4$, magnetization, nanoparticle, surface discharge.

*Corresponding author: L. Sivachandiran, Email: sivachal@srmist.edu.in; sloganat@clarkson.edu

1. Introduction

The preparation of nanomaterials holds tremendous promise across diverse scientific and technological domains, including drug delivery, electronics/optics, catalysis, antibacterial agents, and more, owing to their exceptional properties. Magnetically active nanoparticles (MNPs) have demonstrated significant potential in various fields due to their magnetic, electronic, physical, and chemical characteristics [1].

Among the MNPs, spinel cobalt ferrite ($CoFe_2O_4$) has found widespread applications such as magnetic hyperthermia [2], drug delivery [3], magnetic resonance imaging [4], recyclable nano catalysts [5], and biosensors [6]. In comparison to other spinel ferrites, $CoFe_2O_4$ NPs exhibit high magneto-crystalline anisotropy [7], high coercivity, moderate saturation magnetization (MS), excellent chemical stability, and mechanical hardness at room temperature [8].

The magnetic property of $CoFe_2O_4$ particles is influenced by their size, shape, and purity. Thus, the synthesis step is a crucial for the final product's magnetic characteristics. Various methods for $CoFe_2O_4$ synthesis have been reported, including coprecipitation, sol-gel combustion, solvothermal, microemulsion, mechanical milling, and hydrothermal methods [9]. Among these methods, coprecipitation is widely used for its ability to form high-purity, homogeneous, and crystalline NPs without demanding complex equipment or hazardous materials [10].

Previous studies have highlighted the significance of the synthesis method, annealing temperature, and treatment time in controlling the crystallite size and magnetic properties of $CoFe_2O_4$ [11]. Sundararajan et al. synthesized $Co_{1-x}\ Zn_x\ Fe_2O_4$ nanostructures using the microwave combustion method with L-arginine as fuel, achieving crystallite sizes of 32-45 nm. These structures, confirmed by XRD and Rietveld refinement, exhibited varying magnetic properties, with magnetization (Ms) decreasing from 65.84 to 9.87 emu/g at x=0.1 and increasing from 42.49 to 59.42 emu/g at x=0.2 to 0.5 [12]. In another study, the same authors synthesised $Co_{1-x}Zn_xFe_2O_4$ using urea, resulting in crystallite sizes of 3.07-11.30 nm and band gaps decreasing from 2.56 to 2.17 eV as the Zn content increased. These ferrites exhibited soft magnetic properties, with magnetization (Ms) ranging from 14.26 emu/g (pure $CoFe_2O_4$) to 29.61 emu/g ($Co_{0.7}Zn_{0.3}Fe_2O_4$) [13].

However, the traditional high-temperature calcination process, typically conducted in electrically heated furnaces, poses energy efficiency challenges. The magnetic anisotropy of cobalt ferrite nanoparticles, synthesized through the combustion reaction, has been studied, revealing a significant dependence on both reaction temperature and cobalt concentration [14].

Consequently, there is a growing interest in utilizing various plasmas for material preparation to enhance size and structure control, leading to improved catalytic properties. Non-thermal plasma (NTP), a partially ionized gas with highly reactive species such as ions, electrons and radicals. These active species yield catalysts with unique characteristics compared to those prepared using traditional thermal methods [15]. NTP, includes various types such as microwave discharges (MW), radiofrequency discharges (RF), direct current and alternating current glow discharges (GD), dielectric barrier discharges (DBD), and corona discharges [16].

This study reports the utilization of NTP discharge, specifically DBD plasma, to synthesis materials at low temperature, resulting in noteworthy magnetic properties and reduced band gaps. Cobalt ferrite ($CoFe_2O_4$) nanoparticles were synthesized by *(i)* calcination at 600 °C (CF-C-600), and *(ii)* plasma treatment at 200 °C (CF-P-200). The resultant samples underwent comprehensive characterization through magnetic measurements, UV, SEM, TEM, and XRD analyses. Magnetic properties were examined using a vibrating sample magnetometer (VSM). The adoption of DBD plasma for material synthesis not only showcases potential breakthroughs in materials science but also holds significant promise for the development of advanced materials with versatile applications across diverse industries.

2. Experimental

2.1. Material synthesis

Analytical-grade chemicals were purchased from Sisco Research Laboratory, India, and used without further purification. The co-precipitation method was used to prepare cobalt (II) hydroxide and iron (III) hydroxide. 2 mmol of ferric nitrate ($Fe(NO_3)_3.9H_2O$) and 1 mmol of cobalt nitrate ($Co(NO_3)_2.6H_2O$) were dissolved in 200 ml of distilled water under continuous stirring. To that, 10 ml of 5% NaOH solution was added dropwise with constant mixing. The resulting precipitate was centrifuged and washed using distilled water then dried overnight at 60°C in a hot air oven [17]. The dried precipitate was treated by the following procedures: *(i)* calcined under air at 600°C for 5 h (CF-C-600), and *(ii)* treated by plasma discharge at 200°C for 30 min (CF-P-200).

2.2. Plasma reactor and experimental setup

A detailed description of the quartz tubular reactor and plasma discharge ignition conditions were reported elsewhere [18]. A cylindrical quartz reactor is consisting of 60 cm length, outer diameter (OD) of 2.5 cm, wall thickness of 0.3 cm, and an inner diameter (ID) of 1.9 cm. A high-voltage electrode made of stainless steel with 1.2 cm OD was centered in the middle of the quartz tube, which leads to 0.35 cm discharge gap. The discharge length was fixed at 10 cm by wrapping stainless steel mesh around the quartz tube. The step-up transformer was used to generate the plasma discharge (Jayanti Transformer, Chennai, India). Electrical parameters were determined using two high-voltage probes with a 1:100 attenuation ratio (Zeal Manufacturing Service Limited, Pune, India), which were connected to an oscilloscope (Keysight, 70 MHz 2 Ga s^{-1}) in accordance with Fig.1. The applied and discharge voltage, within the reactor, was determined utilizing the Lissajous method [19].

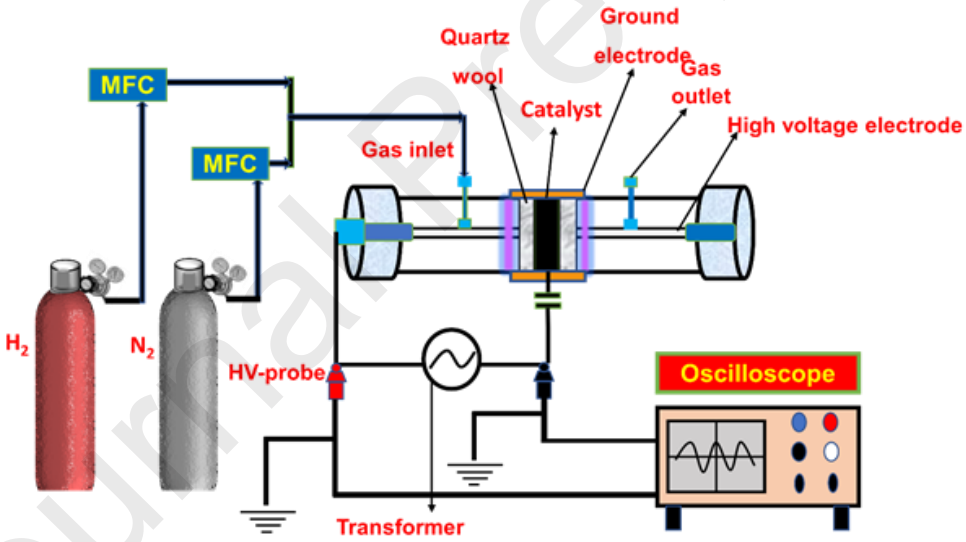

Fig.1. General schematic diagram of the experimental setup.

2.3. Plasma assisted material synthesis

About 0.5 g of prepared material (cobalt (II) hydroxide and iron (III) hydroxide) was loaded in the middle of the quartz reactor (Fig. 1). To ensure most of the material is exposed to plasma discharge, the material was dispersed in quartz wool, sandwiched, and placed in the reactor. For the material synthesis, ultra-pure gases (5% H_2/N_2, 99.999%, Rana Industrial, Chennai) was employed. The total gas flow rate was fixed at 100 mL/min using calibrated mass flow controllers (MFC, KOFLOC, Japan) unless otherwise mentioned. Before igniting plasma discharge the furnace was pre-set at 200°C, and maintained for 30 min. Subsequently, the plasma was ignited using input voltage of 16 kV and frequency of 50 Hz (the corresponding power is 2.5 W) and conditions sustained for 30 min, and the material labelled as **CF-P-200.** It is noteworthy to mention that, to prevent any electrical interference, the furnace

was turned off during the plasma treatment. Despite this precaution, a temperature difference of approximately ±10°C was observed before and after the plasma treatment.

2.4. Material synthesis by calcination

As synthesized material (cobalt (II) hydroxide and iron (III) hydroxide) was calcined at 600°C under 5% H_2/N_2 (100 mL/min total flow). The tubular furnace temperature was raised with the ramp of 10°C/min and maintained at 600°C for 5 h. Then, the furnace was cooled down to room temperature. The synthesised material was labelled as **CF-C-600.**

2.4. Material characterization

The crystal structure was analysed using a PANalytical Xpert3 X-ray diffractometer (XRD, 40 kV, 40 mA, Cu-Kα (1.54 Å) radiation, scan rate of 1°/min and a time of 0.5 s/step). Particle size was determined through High-Resolution Transmission Electron Microscopy (HR-TEM, JEOL Japan JEM-2100 Plus instrument). The secondary electron (SE) imaging mode was used to obtain detailed surface and compositional information. The images were captured in dark-field (DF) modes to enhance contrast and provide different perspectives on the sample's structure. The particle morphology was analysed using field-emission scanning electron microscopy (FE-SEM, Thermo Scientific Apreo S, USA), and the composition was assessed using energy-dispersive spectroscopy (EDS). The measurements were conducted at room temperature under high vacuum conditions, with an acceleration voltage of 20 kV. Imaging was performed using a secondary electron detector. Surface elemental composition and the electronic state of surface elements were examined using X-ray Photoelectron Spectroscopy (XPS, PHI Versaprobe III/Physical Electronics system). Data collection was performed at room temperature using monochromatic Al-Kα radiation (1486.6 eV) as the X-ray source. The analysis was conducted in the high-vacuum mode with a base pressure of approximately 10^{-9} Torr. Survey scans were recorded over a binding energy range of 0-1100 eV at a pass energy of 117.4 eV, with a step size of 0.1 eV. The Ultraviolet-Visible (UV-Vis) spectrophotometer (SHIMADZU, UV 3600 PLUS) was employed to measure material absorbance and understand its optical properties. Magnetic properties of the material were measured using a Vibrating Sample Magnetometer (VSM, Lake Shore) at 300 K. The magnetic hysteresis loops were recorded in a magnetic field range of ±10,000 Oe. The measurements were performed with a sensitivity of 10^-6 emu and a maximum field change rate of 100 Oe/s.

3. Results and discussion

The crystal structure of nanoparticles plays a pivotal role in determining their physical, chemical, and magnetic properties. To gain insights into the crystal structure of the synthesized $CoFe_2O_4$ nano particle, X-Ray Diffraction (XRD) analysis was utilized. As illustrated in **Fig. 2** (a), the XRD pattern of CF-P-200 and CF-C-600 samples unequivocally confirmed the presence of the pure cubic spinel $CoFe_2O_4$ phase, consistent with JCPDS card No. 22.1086. The diffraction pattern revealed well-matched peaks corresponding to characteristic reflections such as (1 1 1), (2 2 0), (3 1 1), (2 2 2), (4 0 0), (4 2 2), (5 1 1), (4 4 0), and (5 3 3) at respective 2θ positions. These reflections confirm the formation of $CoFe_2O_4$ with a cubic spinel structure, specifically characterized by the Fd-3m space group. The Fd-3m space group indicates a face-cantered cubic structure with a high degree of symmetry [12]. In this structure, cobalt ions typically occupy the octahedral sites, while iron ions are distributed between the octahedral and tetrahedral sites of the spinel lattice [13]. The distinct planes and peaks verified the formation of the spinel structure. It is reasonable to infer that 30 min plasma treatment efficiently converted cobalt and iron hydroxide to cobalt ferrite ($CoFe_2O_4$) [20].

Interestingly, the diffraction peaks exhibited increased sharpness and narrowing with high calcination temperature. The crystallite size (D) was estimated from the intense peak, particularly (3 1 1), for both plasma-treated and calcined samples using the Debye Scherrer formula (Equation 1).

$$\boldsymbol{D = \frac{0.89\times\lambda}{\beta\times cos\theta}} \qquad \textbf{Equation 1}$$

where λ is the wavelength of Cu-kα radiation (λ = 1.54 Å), β and θ are Full width at Half Maximum (FWHM) and diffraction angle, respectively [21]. Significantly, the crystallite size increased from 12.4 nm (CF-P-200) to 21.8 nm (CF-C-600). The XRD data strongly support the conclusion that plasma treatment at 200°C for 30 min resulted in a smaller crystallite size compared to samples calcined at 600°C. Moreover, the CF-P-200 sample exhibited broader peaks compared to the CF-C-600 sample, indicating the nanocrystal phase. This suggests that the reduced crystallite size could enhance optical and catalytic properties.

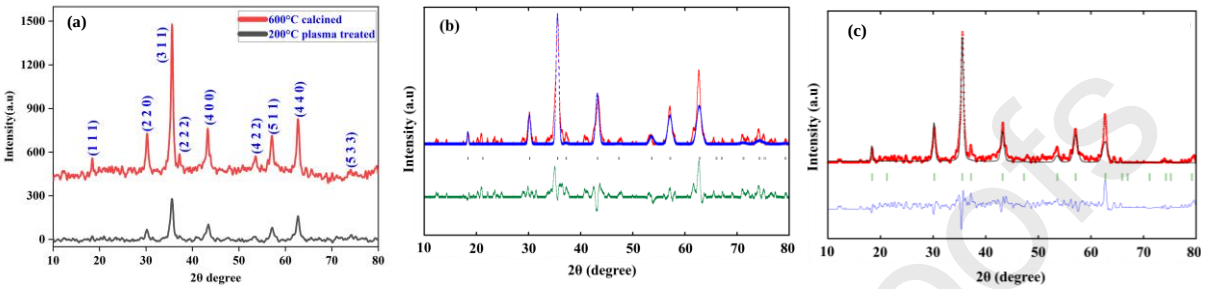

Fig. 2. (a) XRD patterns of plasma treated at 200℃ (CF-P-200) and calcined at 600°C (CF-C-600), (b) Rietveld refined XRD patterns CF-P-200, and (c) CF-C-600. Plasma treatment conditions: 16 kV, and 50 Hz.

Rietveld refinement analyses were performed for plasma treated (CF-P-200) and calcined (CF-C-600) samples using FULLPROF program and reported in *Fig. 2* (b) and (c), respectively [22]. The refinements were performed for the Fd-3m space group. The measured XRD patterns of the plasma-treated and calcined samples were in line with the calculated patterns, and no new phases were observed. The bottom curve suggests that the observed patterns matched with the inverse spinel structure [23].

The surface morphology and particle size of the material were characterized using HR-TEM, and the results are presented in **Fig. 3**. The CF-C-600 sample exhibits a nearly hexagonal shape [24] with an average particle size of 24.1 nm. This value is consistent with the average crystallite size calculated using Debye-Scherrer formula (21.8 nm). However, in the plasma-treated sample, a noticeable reduction in particle size is evident, with an average particle of 6.7 nm, which is about 3.5 times smaller than calcined sample. This small particle size of $CoFe_2O_4$ may be correlated with the surface defects induced during plasma treatment. These defects encompass vacancies, dangling bonds, and structural rearrangements at the atomic or molecular scale [25]. When surface defects are created, they weaken the bonds that hold particles together. Consequently, small particles are formed [26,39]. While the crystallinity is not fully achieved within a 30-min plasma treatment, the process results in the formation of small nanoparticles. Therefore, it can be inferred that adjusting plasma treatment conditions, such as time, plasma input power, and gas composition, could enhance crystallinity while maintaining a small particle size.

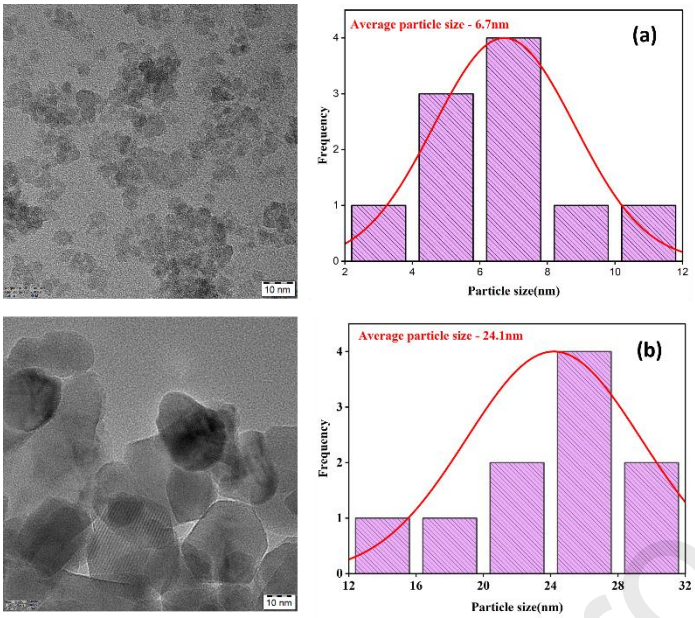

Fig. 3. HR-TEM images of (a) CF-P-200 and (b) CF-C-600.

The results reveal the uniform formation of hexagonal particles, suggesting the potential for $CoFe_2O_4$ nanoparticles to possess high magnetic properties [27]. In conclusion, the plasma treatment significantly influences the formation of $CoFe_2O_4$ nanoparticles. Consequently, the study emphasises the efficacy of plasma treatment at low temperatures in modifying and optimizing the magnetic characteristics of the material.

Furthermore, to compare the surface topography of spinel $CoFe_2O_4$ nanoparticles SEM/EDX spectroscopy was used and the images are reported in **Fig. 4**. It is evident from both images that large particles are present on the surface owing to agglomeration. This clustering is likely the result of magnetic interactions among ferrite nanoparticles stemming from their inherent magnetic properties. Additionally, the bonding of primary particles due to weak surface forces like van der Waals interactions contributes to this agglomeration phenomenon. Notably, the sample treated with plasma demonstrates larger particle dimensions compared to samples subjected to thermal calcination [28,29].

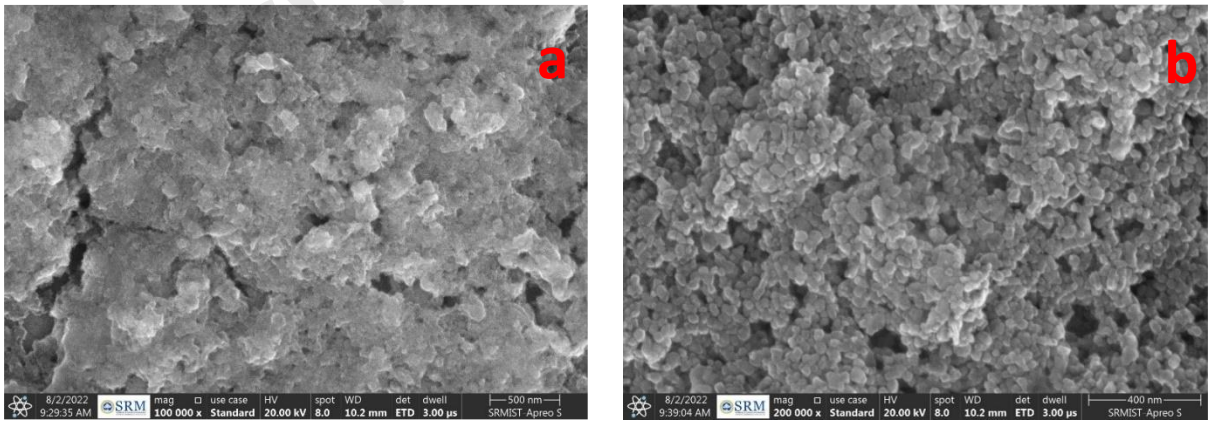

Fig. 4. FE-SEM images of (a) CF-P-200 and (b) CF-C-600.

The surface elemental compositions of the materials were examined through EDX spectroscopy, and the results are reported in

Fig. 5 and summarized in **Table 1**. It was noted that the elemental composition remained consistent across the samples.

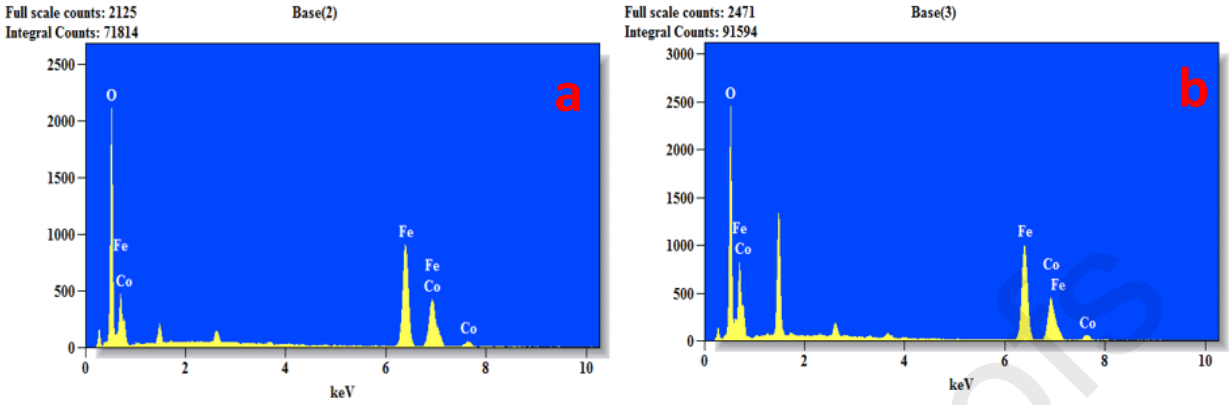

Fig. 5. EDX analysis of (a) CF-P-200 and (b) CF-C-600.

Table 1. Chemical composition of $CoFe_2O_4$ nanoparticles prepared by different process.

Atomic (%)		
Elements	**CF-P-200**	**CF-C-600**
O	**61.19**	**62.21**
Fe	**25.54**	**25.21**
Co	**13.27**	**12.58**
Total	**100**	**100**
Fe/Co	**1.92**	**2.00**

As shown in **Table 1**, both CF-P-200 and CF-C-600 samples displayed nearly identical elemental compositions. However, the plasma-assisted synthesized material exhibited a surface with a lower oxygen content and a higher concentration of metals. Specifically, the Fe^{+3}:Co^{+2} ratio for the plasma-treated material was 1.92, and this value is in good agreement, within the experimental uncertainty, with the expected 2:1 ratio [30]. On the other hand, the Fe^{+3}:Co^{+2} ratio for the calcined sample confirms the presence of the spinel structure. These findings underscore the fact that a 30-min plasma treatment at and 200°C is adequate for achieving nanoparticles with a spinel structure.

Fig. 6 shows the X-ray photoelectron spectra for the surface of $CoFe_2O_4$, prepared through plasma treatment. The low-resolution spectrum is reported in **Fig 6 (a),** revealing the presence of all constituent elements. Deconvoluted high-resolution spectra are reported in **Fig. 6 (b-d)**. For O 1s (**Fig. 6 (b)**), two distinct peaks emerge at approximately 529.7 eV (O_I) and 531.1 eV (O_{II}), corresponding to O-M-O and

vacancy oxygen on the surface, respectively [31]. No other oxygen state associated with adsorbed water or OH ions on the surface are present, indicating that 30 min plasma treatment has efficiently converted metal hydroxide into metal oxides.

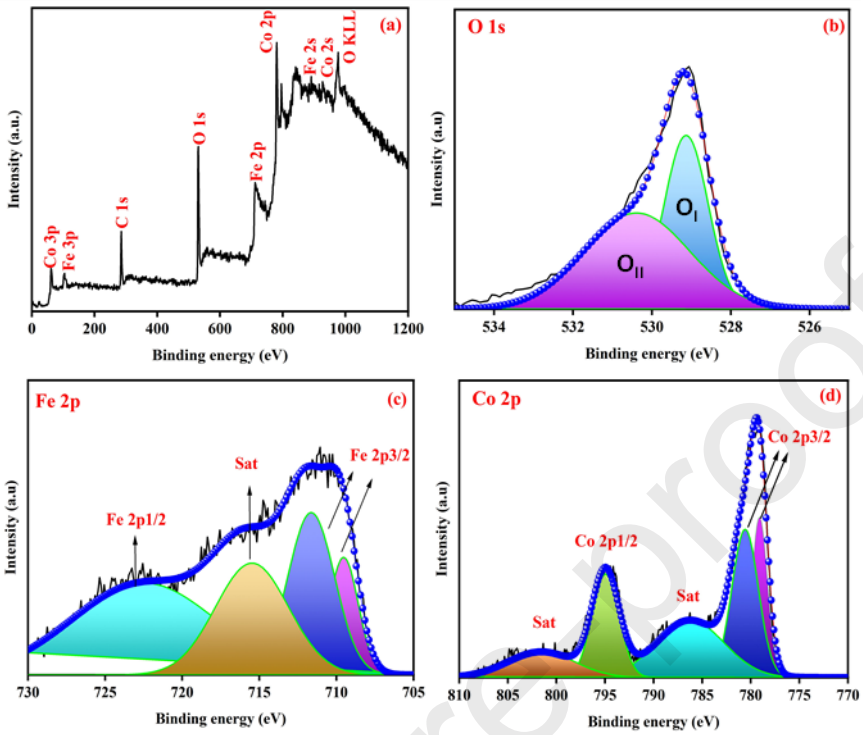

Fig. 6. XPS spectra of CF-P-200, (a) full scan, (b) surface oxygen, (c) Fe 2p and (d) Co 2p.

In **Fig. 6(c),** the Fe 2p spectrum is reported, revealing three distinct peaks. The broad peak, centred at 709.5 eV, can be deconvoluted into two Fe 2p3/2 peaks, which are attributed to multiple Fe^{3+} and Fe^{2+} oxidation states, respectively. Additionally, supporting the existence of Fe^{3+}, a satellite peak at 715.5 eV is observed [35,32]. These observations corroborate the EDX results reported in **Table 1**, indicating that iron (Fe) predominantly exists in the +3-oxidation state, thereby contributing to the formation of spinel ferrite structures. In the Fe 2p spectrum, peaks corresponding to both Fe^{2+} and Fe^{3+} are observed, with Fe^{3+} predominantly located in octahedral (B-sites) positions and, to some extent, in tetrahedral (A-sites) positions [33].

Deconvoluted high-resolution spectra of the Co 2p series are reported in **Fig. 6(d)**. The Co 2p3/2 and Co 2p1/2 peaks manifest at 779.1 eV (B-site, octahedral occupancy) and 795.1 eV (A-site, tetrahedral occupancy), respectively. Accompanying these is a slightly more intense satellite peak at 786.2 eV, suggesting that the predominant population of high-spin Co^{2+} cations is situated in the octahedral sites (B-site) on the surface of $CoFe_2O_4$. This observation unequivocally confirms the coexistence of Co^{2+} and Co^{3+} cation valence states within the spinel crystal structure of ferrite at both octahedral and tetrahedral sites [34,35]. The XPS analysis of $CoFe_2O_4$ also reveals a cation distribution indication of an inverse spinel structure. This mixed valence state distribution of cobalt, coupled with the prevalence of Fe^{3+}, supports the formation of spinel ferrite structures, which in turn contribute to their stability and magnetic characteristics [36, 13].

The optical characteristics of the sample were assessed through UV-DRS analysis, and the material's energy band gap was determined, and reported in **Fig.** *7*. The absorption coefficient *(α)* was determined using Equation 2. The energy band gap (E_g) of the $CoFe_2O_4$ spinel material was calculated using the Kubelka-Munk model expressed in Equation 3.

$$F(R) = \alpha = \frac{(1-R)^2}{2R} \qquad \textbf{Equation 2}$$

Here, F(R) is the Kubelka–Munk function, α is the absorption coefficient, and R is the reflectance.

$$\alpha h\nu = A\left(h\nu - E_g\right)^n \qquad \textbf{Equation 3}$$

In Equation 3, hν , α, A, and n represent the photon energy, absorption coefficient, material parameters, and transition parameter, respectively, with n=2 denoting indirect transitions. Multiple Wood-Tauc plots were generated by plotting $(\alpha h\nu)^2$ versus photon energy (hν) to ascertain the optical band gap energy E_g [37,38].

The findings unveiled a band gap energy of 1.9 eV for CF-P-200, while the CF-C-600 displayed a band gap energy of 2.1 eV. The lower band gap energy exhibited by plasma assisted synthesised nanoparticles may stem from quantum confinement effects. At the nanoscale, electrons in semiconductors experience confinement, leading to an augmented energy difference between filled and empty states, effectively widening the band gap. However, the observed low band gap in plasma-treated nanoparticles could be attributed to the presence of oxygen vacancy. These vacancies introduce in-gap donor states, thereby reducing the energy gap between the Conduction Band (CB) and Valence Band (VB) [39]. From the particle size distribution and their respective band gap energies, it has been observed that for the plasma treated material, the band gap and particle size decrease due to the surface defects induced during plasma treatment. These observations underscore the effectiveness of employing plasma discharge at lower temperatures for the synthesis of optically active materials. Utilizing low temperatures in material synthesis not only enhances energy efficiency but also offers advantages compared to high-temperature calcination methods.

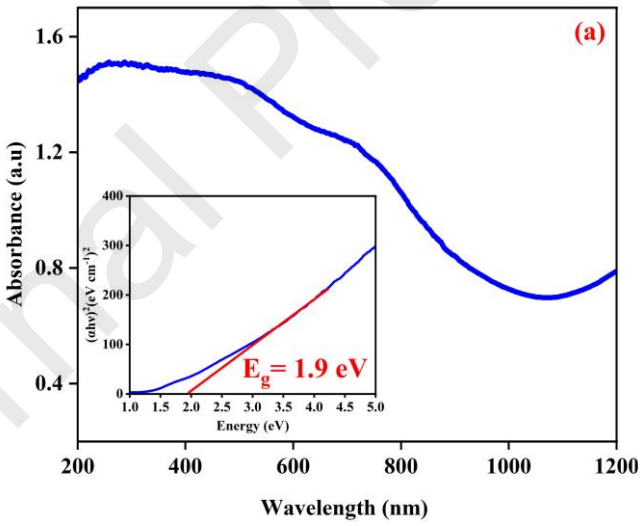

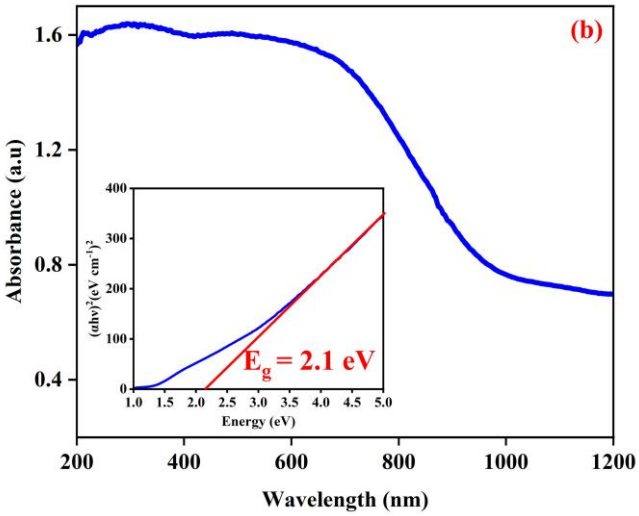

Fig. 7. UV-DRS absorbance of (a) CF-P-200, and (b) CF-C-600. The insert reports the Wood-Tauc plots and band gap calculation.

Magnetic measurements of $CoFe_2O_4$ nanoparticles were performed using the VSM, and the results of magnetic hysteresis measurement at room temperature are shown in ***Fig. 8***. Various studies have investigated the magnetic properties of metal oxide nanoparticles synthesized via different methods. Sundararajan et al. examined $Co_{1-x}Cu_xFe_2O_4$ and noted a decrease in magnetic properties with increasing Cu^{2+} concentration due to cation redistribution, super exchange interaction changes, and lattice defects [23]. Kanithana et al. synthesised Mg^{2+} substituted $NiFe_2O_4$, and reported fluctuations in coercivity, saturation magnetization, and remanence attributed to cation rearrangements and surface imperfections [40]. In another study, Sundararajan et al. synthesized $Co_{1-x}Mg_xFe_2O_4$ nanoparticles, where coercivity initially increased then decreased with Mg^{2+} concentration, while remanence and saturation magnetization generally decreased, attributed to cation redistribution, surface defects, lattice distortions, and magnetic super exchange interactions [22]. Roniboss et al. synthesized MAl_2O_4 (M= Zn and Co) nanoparticles, finding differing coercivity values and remanent magnetization dependent on factors like cationic redistribution, anisotropy, crystallite size, and shape, highlighting the complexity of magnetic properties in these materials [41]. In all these reported works, the synthesized materials were calcined between 500 and 700°C for 1 to 3 h [36]. From the literature it is observed that the method of synthesis, composition of elements effects the magnetization.

As reported in Fig. 8, it is evident that both plasma-treated and calcined samples exhibited ferromagnetism. The saturation magnetization (Ms), retentivity (Mr), coercivity (HC), and magnetic anisotropy (K) values were determined and reported in ***Table. 2***. We observed that subjecting the sample to plasma treatment (CF-P-200) resulted in higher magnetization and lower coercivity (Hc) as compared to the calcined sample CF-C-600 [42].

The magnetic anisotropy (K) is influenced by factors such as degree of crystallinity of nanoparticles, surface area-to-volume ratio, and alterations in inter-particle interactions. The high Ms, and Hc values, and the lower Mr value, are linked to increased magnetic anisotropy of the particles, which prevents magnetic moments from aligning efficiently in an applied field [43]. The ease with which the direction of magnetization reorients to the nearest axis after the removal of the magnetic field is measured by the rectangular ratio (R_S) [42]. The particles interact through magnetostatic interactions, as indicated by R_S value being less than 0.5 [17]. The magnetostatic interactions are responsible for the agglomeration of $CoFe_2O_4$ nanoparticles, as observed in SEM images.

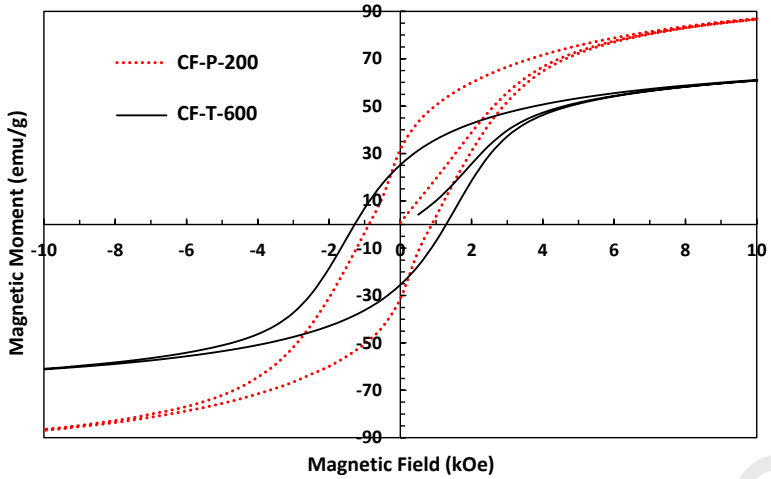

Fig. 8. Magnetic hysteresis at room temperature for sample plasma-treated at 200 °C (CF-P-200) and calcined at 600 °C (CF-C-600).

Table. 2. Saturation magnetization, coercivity, remanence, magnetic anisotropy constant, and rectangular ratio data obtained from magnetic hysteresis loop for plasma-treated and calcined samples.

Sample	Saturation magnetization M_S (emu/g)	Retentivity M_r (emu/g)	Coercivity Hc (Oe)	Magnetic anisotropy K × 10^4 (ergs/cm^3)	Rectangular ratio R_S M_r/M_s
CF-P-200	**91.80**	**31.65**	**888**	**8.49**	**0.34**
CF-C-600	**64.53**	**25.25**	**1289**	**8.66**	**0.39**

This method not only demonstrates energy efficiency but also offers distinct advantages compared to high-temperature methods

Table 3 reports the saturation magnetization (Ms) values for $CoFe_2O_4$ synthesized by various methods and calcination temperatures. Low M_S values have been achieved either by high-temperature (160-1150°C) calcination or prolonged treatment (3 to 20 h). However, similar saturation magnetization has been accomplished by low-temperature (200°C) plasma treatment for a very short duration (30 min). Thus, it can be concluded that using low-temperature plasma discharge to synthesize magnetically active materials is effective. This method not only demonstrates energy efficiency but also offers distinct advantages compared to high-temperature methods

Table 3. Comparison of Saturation Magnetisation (M_S) of $CoFe_2O_4$ material synthesised by various method.

Material	Synthesis method	Temperature	Time	Saturation magnetization (Ms)	Reference
$CoFe_2O_4$	Hydrothermal	160°C	20 h	58.96 emu/g	44
$CoFe_2O_4$	Sol gel combustion method	1150°C	4 h	95.40 emu/g	45
$CoFe_2O_4$	Co-precipitation method	1000°C	4 h	168 emu/g	46
$CoFe_2O_4$	Solvothermal method	160°C	12 h	51.8 emu/g	47
$CoFe_2O_4$	Rosemary-assisted sol-gel method	750°C	3 h	50 emu/g	48
$CoFe_2O_4$	**Co-precipitation/Non-thermal plasma**	**200°C**	**30 min**	**91.8 emu/g**	**In this work**

4. Conclusions

Plasma treatment has demonstrated a favourable influence on the magnetic attributes of $CoFe_2O_4$. This positive transformation is primarily attributed to the alteration of surface composition and morphology facilitated by plasma treatment. The efficacy of this technique lies in its capacity to enhance critical magnetic properties of $CoFe_2O_4$, including magnetic anisotropy, coercivity, and saturation magnetization.

The outcomes derived from applying plasma treatment to cobalt and iron hydroxide materials lay the foundation for extended inquiry in magnetic material synthesis. Exploring the potential of plasma treatment opens the door to creating novel magnetic materials with even enhanced properties. For instance, certain attributes observed in a sample subjected to a 600°C, 5 h calcination process can potentially be replicated through a 200°C plasma treatment in 30 min.

These advancements hold substantial promise across diverse applications, including magnetic data storage, sensors, photocatalysis, and biomedical devices. The ongoing exploration of plasma-treated $CoFe_2O_4$ magnetic materials presents an exciting avenue for future breakthroughs and technological advancements.

ACKNOWLEDGMENT

The authors greatly acknowledge the financial support of the Science & Engineering Research Board, Department of Science & Technology, Government of India (SERB, File No. ECR/2016/001457). We acknowledge SRMIST for the high-resolution scanning electron microscope (HR-SEM) facility. We acknowledge Nanotechnology Research Centre (NRC) and SRMIST for providing the research facilities.

Declarations

Ethical Approval: not applicable

Funding: The authors greatly acknowledge the financial support of the Science & Engineering Research Board, Department of Science & Technology, Government of India (SERB, File No. ECR/2016/001457).

Data Availability: Essential data is provided in the supplementary material, while additional information can be made available upon a reasonable request.

Author Contributions Statement: S.M. H.M. and A.P. designed and performed experiments, drafted the manuscript and figures. N.B., A.A.A., and A.K. edited and refined this manuscript. S.L. conceived, designed, drafted, and edited the manuscript.

All authors contributed to the discussions.

References

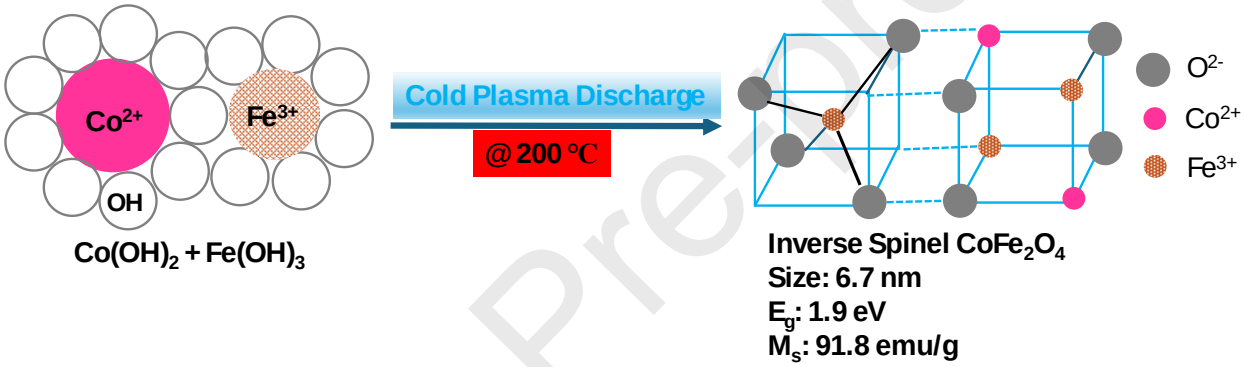

Graphical Abstract

Research Highlights

- A 30-min plasma treatment at 200 °C induced the formation of crystalline particles of inverse spinel $CoFe_2O_4$, a phenomenon not observed in samples without plasma treatment.
- Plasma treatment at 200°C, a significant reduction in particle size was observed, with the average size plummeting to 6.7 nm, nearly three times smaller than the calcined sample at 600°C (24.1 nm).
- The plasma assisted synthesized material displayed remarkable magnetic properties, boasting a magnetization (Ms) of 91.80 emu/g and a coercivity (Hc) of 888 Oe. In stark contrast, the material calcined at 600°C exhibited a lower magnetization of 64.53 emu/g and a higher coercivity of 1289 Oe.
- EDX analysis unveiled surface oxygen defects in plasma synthesized material compared to materials synthesized by conventional calcination at 600°C, resulting in a narrower bandgap (1.9 eV).
- XPS analysis unveiled the presence of Co^{2+} and Co^{3+} within the spinel crystal structure of the plasma-treated material, elucidating the mechanisms underlying its enhanced magnetic behavior.

Declaration of interests

☐The authors declare that they have no known competing financial interests or personal relationships that could have appeared to influence the work reported in this paper.

☒The authors declare the following financial interests/personal relationships which may be considered as potential competing interests:

Sivachandiran LOGANATHAN reports financial support was provided by SRM Institute of Science and Technology (Deemed to be University). Sivachandiran LOGANATHAN reports a relationship with SRM Institute of Science and Technology (Deemed to be University) that includes: employment. If there are other authors, they declare that they have no known competing financial interests or personal relationships that could have appeared to influence the work reported in this paper.

1 S.S. Banifatemi, F. Davar, B. Aghabarari, J.A. Segura, F.J. Alonso and S.M. Ghoreishi,"Green synthesis of CoFe2O4 nanoparticles using olive leaf extract and characterization of their magnetic properties." Ceramics International, 47(13), pp.19198-19204, (2021).

2 E Fantechi, C Innocenti, M Zanardelli, M Fittipaldi, E Falvo, M Carbo, V Shullani, L Di Cesare Mannelli, C Ghelardini, A.M Ferretti, and A Ponti, "A smart platform for hyperthermia application in cancer treatment: cobalt-doped ferrite nanoparticles mineralized in human ferritin cages." ACS nano 8.5, 4705-4719 (2014).

3 M Qasim, K Asghar, and D Das, "Preparation and characterization of CoFe2O4 and CoFe2O4@ Albumen nanoparticles for biomedical applications." Ceramics International 45.18, 24971-24981 (2019).

4 J.I. Kim, C. Chun, B. Kim, J.M. Hong, J.K. Cho, S.H. Lee, and S.C. Song, “Thermosensitive/magnetic poly (organophosphazene) hydrogel as a long-term magnetic resonance contrast platform.” Biomaterials 33(1), pp.218-224 (2012).

5 D. Wang, and D. Astruc. “Fast-growing field of magnetically recyclable nanocatalysts.” Chemical Reviews 114(14), pp.6949-6985 (2014).

6 I. mc Latin-Small-Letter-Dotless, M.Senel, and A. Baykal. "Amperometric hydrogen peroxide biosensor based on cobalt ferrite-chitosan nanocomposite." Materials Science and Engineering. C, Biomimetic Materials, Sensors and Systems 32 (2012).

7 A. Ataie, J. Mostaghimi, L. Pershin, and P. Xu, “Fabrication of nanostructured cobalt ferrite coatings using suspension plasma spraying (SPS) technique.” Surface and Coatings Technology, 328, pp.451-461 (2017).

8 D. Varshney, K. Verma, and A. Kumar, “Substitutional effect on structural and magnetic properties of AxCo1− xFe2O4 (A= Zn, Mg and x= 0.0, 0.5) ferrites.” Journal of Molecular Structure, 1006(1-3), pp.447-452 (2011).

9 S.S. Banifatemi, F. Davar, B. Aghabarari, J.A. Segura, F.J. Alonso and S.M. Ghoreishi,"Green synthesis of CoFe2O4 nanoparticles using olive leaf extract and characterization of their magnetic properties." Ceramics International, 47(13), pp.19198-19204, (2021).

10 M. Houshiar, F. Zebhi, Z.J. Razi, A. Alidoust, and Z. Askari,"Synthesis of cobalt ferrite (CoFe2O4) nanoparticles using combustion, coprecipitation, and precipitation methods: A comparison study of size, structural, and magnetic properties." Journal of Magnetism and Magnetic Materials, 371, pp.43-48 (2014).

11 S. Moosavi, S. Zakaria, C.H. Chia, S. Gan, N.A. Azahari, and H. Kaco, “Hydrothermal synthesis, magnetic properties and characterization of CoFe2O4 nanocrystals.” Ceramics International, 43(10), pp.7889-7894 (2017).

12 M. Sundararajan, V. Sailaja, L. John Kennedy, J. Judith Vijaya, "Photocatalytic degradation of rhodamine B under visible light using nanostructured zinc doped cobalt ferrite: kinetics and mechanism." *Ceramics International* 43, pp. 540-548 (2017).

13 M. Sundararajan, L. John Kennedy, J. Judith Vijaya, U. Aruldoss, "Microwave combustion synthesis of Co1− xZnxFe2O4 (0⩽ x⩽ 0.5): Structural, magnetic, optical and vibrational spectroscopic studies." Spectrochimica Acta Part A: Molecular and Biomolecular Spectroscopy, 140, 421-430, (2015).

14 A. Franco. Jr, and V. Zapf, “Temperature dependence of magnetic anisotropy in nanoparticles of $CoxFe_{(3-x)}O_4$”, Journal of Magnetism and Magnetic Materials, 320, pp. 709-713 (2008).

15 Z. Wang, Y. Zhang, E. C. Neyts, X. Cao, X. Zhang, B. W.-L. Jang, and C. Jun Liu, “Catalyst Preparation with Plasmas: How Does It Work?”, *ACS catalysis,* 8, pp. 2093-2110 (2018).

16 A.H. Khoja, A. Mazhar, F. Saleem, M.T. Mehran, S.R. Naqvi, M. Anwar, S. Shakir, N.A.S. Amin, and M.B. Sajid, “Recent developments in catalyst synthesis using DBD plasma for reforming applications.” International Journal of Hydrogen Energy, 46(29), pp.15367-15388 (2021).

17 M. Basak, M.L. Rahman, M.F. Ahmed, B. Biswas, and N. Sharmin, “Calcination effect on structural, morphological and magnetic properties of nano-sized CoFe2O4 developed by a simple co-precipitation technique.” Materials Chemistry and Physics, 264, pp.124442 (2021).

18 N. Joshi and L. Sivachandiran, “Exploring the feasibility of liquid fuel synthesis from CO_2 under cold plasma discharge: role of plasma discharge in binary metal oxide surface modification.” RSC advances, 11(44), pp.27757-27766 (2021).

19 T.C. Manley, “The electric characteristics of the ozonator discharge.” Transactions of the electrochemical society, 84(1), pp.83 (1943).

20 M. Bououdina, and C. Manoharan, “Dependence of structure/morphology on electrical/magnetic properties of hydrothermally synthesised cobalt ferrite nanoparticles.” Journal of Magnetism and Magnetic Materials, 493, pp.165703 (2020).

21 M.M. Naik, M. Vinuth, K. Karthik, B. Suresh, G. Nagaraju and H.R. Sujatha, “Photocatalytic degradation of dyes by cobalt ferrite nanoparticles synthesized by sol-gel method.” In AIP Conference Proceedings (Vol. 2274, No. 1). AIP Publishing (2020).

22 M. Sundararajan, L. John Kennedy, P. Nithya, J. Judith Vijaya, M. Bououdina, "Visible light driven photocatalytic degradation of rhodamine B using Mg doped cobalt ferrite spinel nanoparticles synthesized by microwave combustion method." Journal of Physics and Chemistry of Solids, 108, pp. 61-75 (2017).

23 M. Sundararajan, and L. John Kennedy, "Photocatalytic removal of rhodamine B under irradiation of visible light using Co1− xCuxFe2O4 (0≤ x≤ 0.5) nanoparticles." Journal of environmental chemical engineering, 5, pp.4075-4092 (2017).

24 G.F. Goya, T.S. Berquo, F.C. Fonseca, and M.P. Morales, “Static and dynamic magnetic properties of spherical magnetite nanoparticles.” Journal of applied physics, 94(5), pp.3520-3528 (2003).

25 S. Nunomura, “A review of plasma-induced defects: detection, kinetics and advanced management." Journal of Physics D: Applied Physics, 56, pp.36 (2023).

26 M.A. Munir, M.S. Naz, S. Shukrullah, M.T. Ansar, G. Abbas, M.M. Makhlouf, "Microwave plasma treatment of NiCuZn ferrite nanoparticles: a novel approach of improving opto-physical and magnetic properties." *Applied Physics A,* 128, pp. 345 (2022).

27 K. Maaz, A. Mumtaz, S.K. Hasanain, and A. Ceylan, “Synthesis and magnetic properties of cobalt ferrite (CoFe2O4) nanoparticles prepared by wet chemical route. Journal of magnetism and magnetic materials,” 308(2), pp.289-295 (2007).

28 N. Hosni, K. Zehani, T. Bartoli, L. Bessais, and H. Maghraoui-Meherzi, “Semi-hard magnetic properties of nanoparticles of cobalt ferrite synthesized by the co-precipitation process.” Journal of Alloys and Compounds, 694, pp.1295-1301 (2017).

29 M. Kurian, S. Thankachan, D.S. Nair, A. EK, A. Babu, A. Thomas, and B. Krishna KT, “Structural, magnetic, and acidic properties of cobalt ferrite nanoparticles synthesised by wet chemical methods.” Journal of Advanced Ceramics, 4, pp.199-205 (2015).

30 M. Fantauzzi, F. Secci, M. S. Angotzi, C. Passiu, C. Cannas, and A. Rossia, “Nanostructured spinel cobalt ferrites: Fe and Co chemical state, cation distribution and size effects by X-ray photoelectron spectroscopy”, RSC Advances, 9, pp.19171–19179, (2019).

31 Y. Zhao, X. Ma, P. Xu, H. Liu, Y. Wang and A. He, “Elemental mercury removal from flue gas by $CoFe_2O_4$ catalysed peroxymonosulfate”, Journal of hazardous materials, 341, pp.228-237 (2018).

32 M. Xu, J. Li, Y. Yan, X. Zhao, J. Yan, Y. Zhang, B. Lai, X. Chen and L. Song, “Catalytic degradation of sulfamethoxazole through peroxymonosulfate activated with expanded graphite loaded $CoFe_2O_4$ particles.” Chemical engineering journal, 369, pp.403-413 (2019).

33 N. Liu, P. Du, P. Zhou, R.G. Tanguturi, Y. Qi, T. Zhang, and C. Zhuang, "Annealing temperature effects on the cation distribution in $CoFe_2O_4$ nanofibers" Applied Surface Science, 532, pp. 147440, (2020).

34 K.L. Yan, J.F. Qin, J.H. Lin, B. Dong, J.Q. Chi, Z.Z. Liu, F.N. Dai, Y.M. Chai, and C. G. Liu, "Probing the active sites of Co_3O_4 for the acidic oxygen evolution reaction by modulating the Co^{2+}/Co^{3+} ratio." Journal of Materials Chemistry A, 6(14), pp.5678-5686 (2018).

35 N. Ballarini, F. Cavani, S. Passeri, L. Pesaresi, A.F. Lee, and K. Wilson, "Phenol methylation over nanoparticulate $CoFe_2O_4$ inverse spinel catalysts: The effect of morphology on catalytic performance." Applied Catalysis A: General, 366(1), pp.184-192 (2009).

36 S. Hunpratub, S. Phokha, P. Kidkhunthod, N. Chanlek, P. Chindaprasirt, "The effect of cation distribution on the magnetic properties of CoFe2O4 nanoparticles." Results in Physics, 24, pp.104112 (2021).

37 M. Sundararajan, L.J. Kennedy, P. Nithya, J.J. Vijaya, and M. Bououdina. "Visible light driven photocatalytic degradation of rhodamine B using Mg doped cobalt ferrite spinel nanoparticles synthesized by microwave combustion method." Journal of Physics and Chemistry of Solids, 108, pp.61-75 (2017).

38 M.A. Almessiere, Y. Slimani, S. Güner, M. Nawaz, A. Baykal, F. Aldakheel, S. Akhtar, I. Ercan, İ. Belenli and B.E.K.İ.R. Ozcelik. "Magnetic and structural characterization of Nb^{3+}-substituted $CoFe_2O_4$ nanoparticles." Ceramics International, 45(7), pp.8222-8232 (2019).

39 P.J. Boruah, R.R. Khanikar, and H. Bailung. "Synthesis and characterization of oxygen vacancy induced narrow bandgap tungsten oxide (WO3−x) nanoparticles by plasma discharge in liquid and its photocatalytic activity." Plasma Chemistry and Plasma Processing, 40, 1019-1036 (2020).

40 S. Kanithan, N. Arun Vignesh, K. Mohammedsaleh Katubi, P. Sarathi Subudhi, E. Yanmaz, J. Arockia Dhanraj, N. Salem Alsaiari, K. M. Abualnaja. M. Sukumar, M. Sundararajan, S. Baskar, S. Sahu, C. Sekhar Dash. "Enhanced optical, magnetic, and photocatalytic activity of Mg2+ substituted NiFe2O4 spinel nanoparticles." Journal of Molecular Structure, 1265, pp. 133289, (2022).

41 A. Roniboss, A. Subramani, R. Ramamoorthy, S. Yuvaraj, M. Sundararajan, C. Sekhar Dash "Investigation of structural, optical and magnetic behavior of MAl2O4 (M= Zn and Co) nanoparticles via microwave combustion technique." Materials Science in Semiconductor Processing, 123, pp. 105507, (2021).

42 S. Joseph Olusegun, E. Tadeu Fraga Freitas, L. Roni Silva Lara, H. Osório Stumpf, N. Della Santina Mohallem, "Effect of drying process and calcination on the structural and magnetic properties of cobalt ferrite." Ceramics International, 45, pp.8734-8743 (2019).

43 M. Gharagozlou. "Synthesis, characterization and influence of calcination temperature on magnetic properties of nanocrystalline spinel Co-ferrite prepared by polymeric precursor method." Journal of Alloys and Compounds, 486(1-2), pp.660-665 (2009).

44 S. Fayazzadeh, M. Khodaei, M. Arani, S. R. Mahdavi, T. Nizamov and A. Majouga Fayazzadeh, "Magnetic properties and magnetic hyperthermia of cobalt ferrite nanoparticles synthesized by hydrothermal method," Journal of Superconductivity and Novel Magnetism, 33, pp. 2227-2233, (2020).
45 T. Wegayehu Mammo, N. Murali, Ch. Vijaya Kumari, S.J. Margarette, A. Ramakrishna, R. Vemuri, Y.B. Shankar Rao, K.L. Vijaya Prasad, Y. Ramakrishna, and K. Samatha, "Synthesis, structural, dielectric and magnetic properties of cobalt ferrite nanomaterial prepared by sol-gel autocombustion technique." Physica B: Condensed Matter, 581, pp. 411769, (2020).
46 M. Basak, Md. Lutfor Rahman, Md. Farid Ahmed, B. Biswas, and N. Sharmin, "Calcination effect on structural, morphological and magnetic properties of nano-sized CoFe2O4 developed by a simple co-precipitation technique." Materials Chemistry and Physics, 264, pp. 124442, (2021).
47 Z. Shi, Y. Zeng, X. Chen, F. Zhou, L. Zheng, G. Wang, J. Gao, Y. Ma, L. Zheng, B. Fu, and R. Yu, "Mesoporous superparamagnetic cobalt ferrite nanoclusters: Synthesis, characterization and application in drug delivery." Journal of Magnetism and Magnetic Materials, 498, pp. 166222 (2020).
48 M. Ghanbari, F. Davar, and A. Esmail Shalan, "Effect of rosemary extract on the microstructure, phase evolution, and magnetic behavior of cobalt ferrite nanoparticles and its application on anti-cancer drug delivery", Ceramics International, 47, pp. 9409-9417, (2021).